Advanced Drug Delivery Reviews 63 (2011) 417–426

Contents lists available at ScienceDirect

Advanced Drug Delivery Reviews

journal homepage: www.elsevier.com/locate/addr

Controlling drug nanoparticle formation by rapid precipitation ☆

Suzanne M. D'Addio, Robert K. Prud'homme *

Department of Chemical and Biological Engineering, Princeton University, Princeton, NJ 08544, USA

ARTICLE INFO

Article history:
Received 19 November 2010
Accepted 22 April 2011
Available online 30 April 2011

Keywords:
Nucleation
Growth
Supersaturation
Antisolvent addition
Flash nanoprecipitation
Nanoparticle
Prodrug

ABSTRACT

Nanoparticles are a drug delivery platform that can enhance the efficacy of active pharmaceutical ingredients, including poorly-water soluble compounds, ionic drugs, proteins, peptides, siRNA and DNA therapeutics. To realize the potential of these nano-sized carriers, manufacturing processes must be capable of providing reproducible, scalable and stable formulations. Antisolvent precipitation to form drug nanoparticles has been demonstrated as one such robust and scalable process. This review discusses the nucleation and growth of organic nanoparticles at high supersaturation. We present process considerations for controlling supersaturations as well as physical and chemical routes for modifying API solubility to optimize supersaturation and control particle size. We conclude with a discussion of post-precipitation factors which influence nanoparticle stability and efficacy *in vivo* and techniques for stabilization.

Contents

1. Introduction

Engineered organic nanoparticles have been investigated for many applications due to the enhanced material properties that result from a reduction in particle dimensions. Perhaps the most active area of research is in the pharmaceutical industry, where drug nanoparticles have the potential to provide customized drug delivery vehicles [1]

☆ This review is part of the *Advanced Drug Delivery Reviews* theme issue on "Nanodrug Particles and Nanoformulations for Drug Delivery".

* Corresponding author. Tel.: +1 609 258 4577; fax: +1 609 258 0211.
E-mail address: prudhomm@princeton.edu (R.K. Prud'homme).

0169-409X/$ – see front matter © 2011 Elsevier B.V. All rights reserved.
doi:10.1016/j.addr.2011.04.005

and targeted probes for bioimaging [2,3]. In recent years, many of the new lead compounds coming from drug discovery efforts are compounds that are difficult to deliver effectively. Examples are compounds with low aqueous solubility and oral bioavailability, as well as newer therapeutics which are sensitive to degradation or opsonization and clearance [4,5]. To enable the use of therapeutic compounds such as these, non-traditional dosage forms and delivery routes have been intensely investigated. Many nano-constructs including liposomes, dendrimers, lipid and polymeric nanoparticles and nanocapsules have been developed in the effort to overcome the aforementioned delivery barriers and their formation as drug nanocarriers is reviewed elsewhere [6–10].

Pure drug nanoparticle delivery systems with high payloads, extended circulation times and active targeting capabilities show particular promise to help realize the potential of new therapeutic entities [1] or to improve the delivery of currently used drugs [11] by increasing the maximum tolerated dose (MTD) [12], limiting systemic distribution of cytotoxic agents [13], protecting from opsonization and clearance in the bloodstream [14,15], increasing dissolution rates and bioavailability [16,17] and localizing drugs by passive [18–20] and/or active targeting [21]. Therefore, there is strong motivation to develop general techniques for the manufacture of therapeutic nanoparticles. In the development of nanoparticle formulations with multiple functionalities, success requires an understanding of the phenomena controlling their synthesis, form and stability. To obtain nanoparticles of drugs, "top-down" processes that involve breaking down larger particles by milling are a relatively simple method to produce nanoparticles [22], while "bottom-up" processes involving assembling and controlling precipitations at the nanometer scale are often more challenging. However, the latter route opens the way for interesting possibilities to incorporate multiple APIs in a single nano carrier and to tailor nanoparticle surface functionality.

The focus of this review is on the assembly and stability of drug nanoparticles *via* supersaturation and precipitation. The nucleation and growth kinetics dictate the final particle size and the size distribution (Section 2) and are controlled via supersaturation, which can be achieved by controlling process parameters (Section 3) and by modifying API solubility (Section 4). The phase of the drug in nanoparticle form (i.e. crystalline or amorphous) affects stability and bioavailability *in vivo* (Section 5). Lastly, the stability of the particles can be affected by aggregation or recrystallization, which is driven by the high energy of the interface, and approaches to stabilizing are described (Section 6).

2. Nucleation and growth

In classical crystallization theory, phase separation occurs at the onset of supersaturation in order to reduce the system free energy. In homogenous nucleation, local concentration fluctuations result in the formation of primary nuclei, which grow by the association/aggregation of molecular species, in a statistical manner, until a critical size is reached and the nuclei are stable against dissolution. The nucleation rate B follows an Arrhenius relationship [23]

$$B = K_1 \, exp\left(-\frac{\Delta G_{cr}}{kT}\right). \tag{1}$$

Here K_1 is a constant, k is Boltzmann's constant, T is the absolute temperature and ΔG_{cr} is the critical free energy for nucleation. The free energy change for nucleation of a spherical particle with radius, r, is the sum of the contributions of the energy required to form an interface, ΔG_s, and the free energy to form the bulk phase, ΔG_v, [24]

$$\Delta G = \Delta G_s + \Delta G_v = 4\pi r^2\gamma + \frac{4}{3}\pi r^3 \Delta G_v \tag{2}$$

where γ is the surface tension. The interfacial term is always positive. Since precipitation only occurs when the solution is supersaturated, the bulk free energy change for precipitation is negative. The critical nucleus size, r_c, comes from differentiating and minimizing this function with respect to the radius,

$$r_c = \frac{-2\gamma}{\Delta G_v} \tag{3}$$

The supersaturation ratio, S_r, is defined as the ratio of the particle solubility at the interface, c_s, to the bulk solubility, c_∞,

$$S_r \equiv \frac{c_s}{c_\infty} \tag{4}$$

and the solubility at the nanoparticle interface is given by the Kelvin equation [25,26], written in terms of the local supersaturation at the particle surface, S_r,

$$ln\, S_r \equiv ln\frac{c_s}{c_\infty} = \frac{2\gamma M}{\rho RTr} \tag{5}$$

where M is the molecular mass of the solute, ρ is the density, R is the gas constant and T is the absolute temperature. The supersaturation at the critical radius, r_c, is then given by the combination of Eqs. (3) and (5).

Substituting Eqs. (3) and (5) in Eq. (2) yields the expression for ΔG_{cr} and B is given by [23]

$$B = K_1 \, exp\left(-\frac{16\pi\gamma^3\upsilon^2}{3k^3T^3[\, ln(S_r)]^2}\right) \tag{6}$$

where υ is the molar volume. Therefore, the nucleation kinetics are controlled through both the local supersaturation and the temperature.

In precipitations, the supersaturation is often not uniform throughout the volume, which leads to some confusion in evaluating the literature. For processes involving precipitation by cooling, the walls of the vessel will be colder than the average vessel volume and so the value of S_r in Eq. (4) becomes spatially inhomogeneous. In solvent-exchange precipitations where a dissolved solute is added to a large volume of non-solvent, the supersaturation is often reported as the total mass of solute added divided by the final solution volume, c, divided by bulk solubility in the final solvent mixture [27]

$$S \equiv \frac{c}{c_\infty}. \tag{7}$$

This definition of supersaturation has no relationship to the actual thermodynamic driving force for precipitation, which happens locally, and changes over time. Mass transfer or mixing limitations in both of these cases may make the actual supersaturation that controls nucleation and growth orders of magnitude smaller than the average value. This distinction becomes important for rapid precipitations at high supersaturation.

Nucleation stops when the growth of earlier nuclei depletes the solution supersaturation. The nuclei continue to grow until the concentration of solute c is at the equilibrium value c_∞. The precise control of nucleation is often difficult, and so "seed" crystals are often added to the system for heterogeneous crystallizations of large sized particles. In heterogeneous nucleation, the inclusion of foreign substrates reduces ΔG_{cr} and thus nucleation occurs at a lower supersaturation with the assembly of molecular species on the substrate. The seeds control the number of particles by acting as the nuclei. The area of large particle crystallization and seeding is outside the scope of this review, but the reader is referred to Mullin [28,29]. Seeding is not viable for the production of nanoparticles because the production of

nanometer-sized seeds would be more challenging than producing 10–100 nm nanoparticles!

As an alternative to seeding to produce API nanoparticles, hydrophobic macromolecules may be used to reduce the activation energy for particle growth, induce nucleation, control the number of nuclei and thus reduce particle size [30]. Saad added homopolymer polycaprolactone (PCL) dissolved with paclitaxel in a water miscible solvent, tetrahydrofuran, to drive heterogeneous nucleation in water. For a series of experiments at constant mass of PCL but with molecular weights of 1250, 2000 and 10,000 g/mol, nanoparticles of 80, 95 and 147 nm, respectively, were produced. There are fewer PLC chains at higher molecular weight and therefore fewer nuclei produced. The drug accumulates on the fewer nuclei and produces larger particle sizes. This area of heterogeneous nucleation to control nanoparticle formation is largely unexplored at this time.

The relative kinetics of nucleation and growth dictate the quality of the final particle size distribution. In the rapid precipitation of pharmaceuticals, Mahajan and Kirwan explored the nucleation and growth kinetics of lovastatin at low and high supersaturations, ranging from $S = 1.8$ to 7.4 in the absence of mixing limitations by using a grid mixer with a quantified mixing time of 3 ms [31]. The grid mixer does not suffer from the problem of spatially dependent supersaturation, as described above for batch crystallizations, because all of the solute is rapidly and uniformly mixed within 3 ms in a known fluid volume. The results are summarized in Fig. 1. As expected, the nucleation rate is found to increase with increasing supersaturation. Further, as supersaturation increases, both the nucleation rate and growth rate undergo a distinct transition, corresponding to a transition from heterogeneous to homogenous nucleation. In the high supersaturation regime, secondary nucleation is largely avoided and formation of nuclei is favored prior to significant growth, since the rate at which the nucleation rate increases is four orders of magnitude greater than that for the growth kinetics.

To gain insight on the growth mechanism for the nuclei, growth models were fit to the experimental data. While a number of theories exist for the mechanism of growth of a crystal face [31], in general, it is most energetically favorable for a molecule to desolvate and incorporate on a growing crystal with a maximum number of contacts at a kink site, rather than on the surface of a growing face or at the edge of a growing face. A new crystal face then grows by absorption and diffusion of solute particles. At high supersaturations and in the absence of transport limitations, a surface nucleation growth mechanism best fits the data of Mahajan and Kirwan. Therefore, the rate of particle growth, G, is limited by the incorporation of molecules at kink sites and surface growth of "steps" across the surface, which develop by a polynuclear nucleation mechanism on the face of the growing crystal [31].

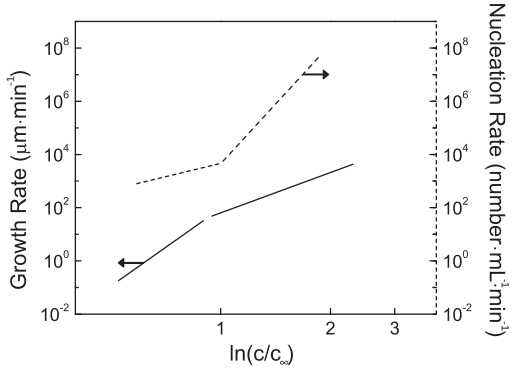

Fig. 1. The nucleation and growth rate of lovastatin crystals as a function of supersaturation. At low supersaturation, the growth rate increase dominates the changing precipitation kinetics. However, after a transition from heterogeneous nucleation to homogenous nucleation, the rate of increase in the growth rate decreases and the nucleation rate increases dramatically. Adapted from [31].

3. Creating supersaturation

Understanding the influence of supersaturation on particle nucleation and growth has motivated the development of techniques which are capable of optimizing supersaturation in order to reduce the size and distribution of precipitated particles. In this section, we review the major two processing techniques for inducing supersaturation of drug compounds. Traditionally, temperature quenching has been applied to create micro-scale powders with narrow size distributions while antisolvent addition has emerged as an approach to achieve much high supersaturations for the production of nanoparticles.

3.1. Temperature quenching

In the preparation of traditional dosage forms, the precipitation of drug crystals is a critical step after chemical synthesis in which the crystal polymorph, purity and size are determined. Supersaturation and crystallization of drug compounds is often accomplished on an industrial scale by cooling saturated drug solutions to induce supersaturation in batch or semibatch processes. Open loop temperature control of cooling profiles is most often used to control the particle size distribution, though sophisticated control of the supersaturation under the metastable zone limit has been shown to be an alternative route to limiting polydispersity [32–34].

These techniques for crystallization of drug compounds are unsuitable for the production of exclusively nanoscale drug particles. The supersaturations that can be obtained by cooling a vessel are not spatially uniform and are typically low [31], where values of $S = 10$ are considered high [35]. In contrast, supersaturations of 10,000 have been achieved for solvent-switching and micromixing [36]. The cooling applied at the walls of a crystallization vessel induces local API nucleation in fluid which is then convected by mixing into the bulk of the solution. Additional nuclei are formed by further convection of fluid which creates a continuous process of nonuniform nucleation, subsequent growth and yields a broad distribution of particle sizes. In the Chemical Engineering field, this would be termed the "residence time distribution" problem.

Supersaturation reached in this way is also limited by the thermal stability of the drug. While traditional small molecule drugs are more robust, newly developed biological therapeutic compounds are not amenable to heating and cooling cycles. Thus, while temperature quenching to induce supersaturation is viable for traditional crystallization processes, new technologies to robustly produce nanoparticles are required.

3.2. Antisolvent addition

An alternative technique to temperature quenching is the addition of an antisolvent to the API solution to reduce solubility, or the reverse, diluting the dissolved API into an antisolvent [37–40]. In this way, mild temperatures may be maintained and supersaturations high enough to yield nanoparticles are attainable. For hydrophobic APIs, self assembly is initiated *via* a change from organic media to a poor solvent, such as water or an aqueous buffer, while precipitation has been accomplished for water-soluble compounds *via* addition of a organic solvent [41,42]. Though high supersaturation decreases both the size of the critical nucleus r_c and increases the nucleation rate B, it demands processes with very short characteristic mixing times to ensure a suitable particle size distribution. A review of mixing technologies by Johnson and Prud'homme details the development of improved mixing technologies which have enabled the use of anti-solvent addition to

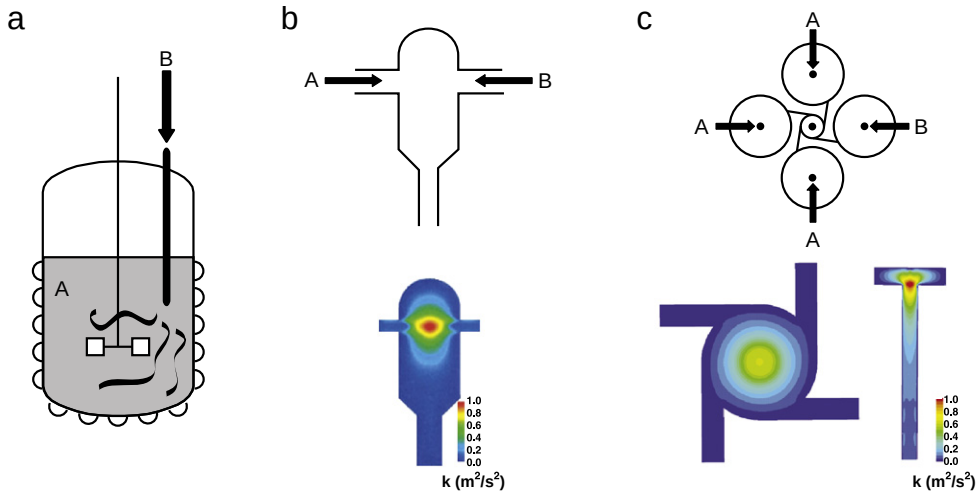

Fig. 2. Anti-solvent precipitation geometries: (a) batch and (b–c) continuous confined mixing geometries. In each schematic, B represents the water-miscible organic stream with the dissolved API. The anti-solvent (typically water) is A. For the batch mode, the vessel is initially filled with A, whereas in the continuous precipitation geometry the A stream is continuously injected with the B stream. Fluid dynamics simulations reveal that (b) for the CIJ, the highest energy mixing occurs at the collision of the impinging streams, whereas (c) in the MIVM, this point of highest energy occurs at the exit of the mixing chamber. Figure adapted from references [43,48]. Color version available online.

achieve high supersaturation and nucleation under homogenous conditions [43].

There are two modes of operation for anti-solvent precipitation: batch and continuous confined flow, as depicted in Fig. 2. For simplicity we will consider the case of hydrophobic actives that are precipitated by the addition of water as the anti-solvent. In the batch processes, the API in a water-miscible organic solvent such as methanol, ethanol, dimethylsulfoxide, tetrahydrofuran, N-methyl-2-pyrrolidone, dimethylformamide or acetone is injected from a small orifice into a vessel which is being rapidly mixed (Fig. 2a) [27,44,45]. Dilution of the organic stream by the bulk water initiates precipitation. To limit particle aggregation and maintain nanometer particle size, a water dispersible polymer is added to the aqueous phase. The polymers most frequently used are polypropylene oxide-polyethylene oxide block copolymers (Pluronics® or Poloxamers®), polyvinyl alcohol or polyvinyl caprolactones. This process has the advantage of using existing batch vessels but has the disadvantage of poorer mixing than in the continuous confined geometries and, therefore, less control of particle size and generally produce larger sized particles.

We will focus on the newer approach of continuous confined precipitation geometries (Fig. 2b and c). As shown in Table 1, the advantage of these geometries is that higher mixing intensities can be achieved by these mixers with shorter characteristic mixing times. In these processes, the antisolvent stream and the organic solvent stream containing drug and the stabilizing polymer are brought together in a confined mixing chamber. The geometry may involve two streams injected into a cavity, which has taken the name "confined impinging jet" (CIJ) mixers (Fig. 2b) [43,46]. A variation of the impinging jet geometry is coaxial flow of the two streams [47] but has poorer mixing efficiency than impinging jets. The mixing time in a CIJ mixer has been quantified to demonstrate that mixing times on the order of milliseconds can be achieved [43]. The mixing in a CIJ requires the use of streams of equal momentum which impinge upon each other, dissipating their momentum upon collision, resulting in efficient micromixing. The requirement for equal momentum limits the control over supersaturation that can be achieved.

Table 1
Approximate energy dissipation rates for process equipment. The rate of mixing two fluids in turbulence increases as the energy dissipation rate increases. The data in the table is compiled from the work of Bourne and coworkers from a variety of sources [106–109].

Method	Energy dissipation	Comments
Impinging jets	1000–100,000	Based on momentum balance
Single turbulent jet	1000–40,000	Peak, large spatial variation
Rotor-stator mixer	500–5000	Peak near rotor
Static mixers	10–500	Inject in elements
Stirred tank	0.1–33	Depending on position
Centrifugal pumps	1	In volute
Turbulent pipe	1	0.1 axis, up to 10 near wall

The other class of geometries involves multiple streams that are directed into a central cavity (Fig. 2c) which has taken the name, "multiple inlet vortex mixers" (MIVM) [48]. The flows into the confined mixing chamber are continuous and the time scale for mixing is well defined. All of the fluid elements pass through the high energy mixing zone and experience the same history. Mixing in the chamber has been characterized using competitive fast reactions and it was shown that homogenous conditions were achieved in the mixing chamber when the Reynolds number is >1600 [48].

The inserts in Fig. 2b and c for the CIJ and MIVM mixers are computational fluid mechanics calculations of the energy dissipation rates in the mixers [46,48]. In the CIJ, the highest energy density is in the center of the cavity, whereas the MIVM has the highest energy density at the exit port of the chamber. Production volume is determined by time that the process operates, rather than the volume of the batch vessel. These jet mixers scale from laboratory to production sized devices, whereas the scale up of batch mixers to larger volumes is generally difficult for nanoparticle precipitation [43].

Antisolvent precipitation using confined mixing geometries has been applied to the production of complex and multifunctional therapeutic nanoparticles, including proteins and peptides [49], imaging agents and therapeutics [50,51], and composite nanoparticles with organic and inorganic cores [52,53]. When multiple streams are used, it is possible to separate drugs, excipients and/or stabilizers which may not all be miscible in the same solvent. Supersaturation according to Eq. (7) can be controlled through (1) the concentration c of drug in the system and (2) the drug solubility c_∞ after mixing through the quality of the mixed solvent. The flexibility of the MIVM allows for control over the solvent mixing ratios through relative flow rates, due to the fact that all streams contribute independently to mixing in the chamber, and thus a wide range of values of c_∞ can be reached.

To determine the optimal solvent/antisolvent mixing ratio for supersaturation (e.g. volumetric flow ratio) in a precipitation process, a supersaturation curve can be constructed as shown in Fig. 3. The data in Fig. 3 are calculated from the measured solubility c_∞ versus solvent composition data and Eq. (7). The solubility at each solvent composition is determined by preparing a saturated solution of the active in a 100% organic solution, which is then mixed as the indicated volume ratios and allowed to equilibrate. The precipitated drug is filtered out and the remaining drug in solution is quantified.

The commercial pesticide Boscalid (BASF) has an equilibrium water solubility of 5 μg/L and a solubility in THF of 2.3×10^8 μg/L. In Fig. 3a, at too low a mixing ratio of water to solvent, low supersaturations are achieved due to inadequate reduction in c_∞. As the volume fraction of the solvent is decreased, the supersaturation increases dramatically, reaching nearly 1000 at 5 vol.% organic. Beyond 5%, very high ratios of water to solvent dilutes the drug concentration, c, so that, despite low solubility c_∞, the supersaturation is low. The competition between c_∞ and c results in a maximum supersaturation. For a compound such as Peptide B, a 7 residue model peptide, that has a considerably higher water solubility of 10 mg/L [49] and a solubility of 2×10^5 mg/L in a 50/50 (v/v) mixture of DMF and NMP, the maximum attainable supersaturation is only 3 at 30 vol.% organic. The data for these systems indicates that the value of the maximum supersaturation and the corresponding mixing ratio depends on the solubility of the solute of interest in the particular solvent/anti-solvent system. The latter parameter can be optimized through the construction of solubility curves in several solvents, while the solubility of the solute in a solvent system may be tailored through means described in Section 4.

In addition to adjusting the solvent quality *via* mixing ratios, the supersaturation depends on solute concentration, c. The highest supersaturation is achieved by saturating both streams prior to mixing. When the concentration of API in the organic stream is decreased from saturation to 20× below the equilibrium solubility in the organic phase, $c_{\infty,\ organic}$, the supersaturation drops, so that supersaturation is only attainable at a limited range of solvent compositions as shown in Fig. 3b for Boscalid.

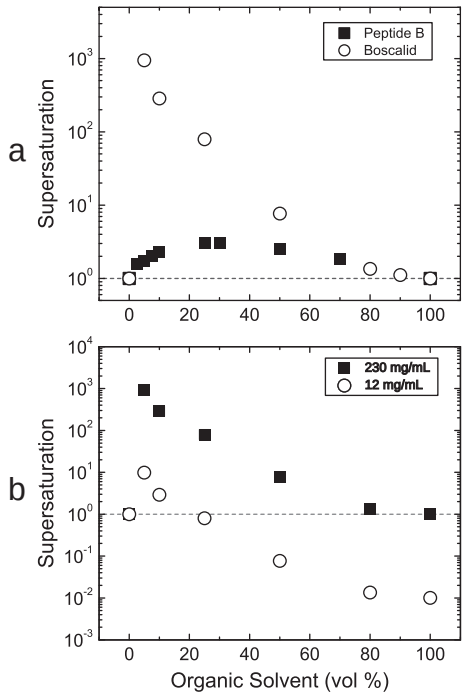

Fig. 3. Supersaturation, S, as a function of the relative mixing ratios of organic solvent to water. (a) Comparison of highest attainable supersaturation for (○) Boscalid, a pesticide, and (■) Peptide B, a seven residue model peptide. The organic stream contains Boscalid at a concentration of 230 mg/mL and Peptide B at 200 mg/mL, their saturation concentrations. There is a maximum superpersaturation that depends on each API/solvent system. (b) When the concentration of Boscalid in the organic stream is decreased 20-fold, the conditions at which supersaturation and nanoprecipitation is achieved becomes limited.

4. Methods for supersaturating therapeutic compounds

In cases where water solubility limits supersaturation, it may be desirable to modify the hydrophobicity of a drug compound to increase supersaturation in aqueous media to facilitate nanoparticle formation and stabilization. We now describe the modifications to therapeutic agents which may be applied to increasing the hydrophobicity of poorly water soluble, hydrophilic, ionic and inorganic therapeutic agents.

4.1. Increasing hydrophobicity by covalent conjugation

Conjugation of a drug compound to a poorly-soluble "anchor" (i.e. a hydrophobic compound to which it can be conjugated) results in a prodrug that will have decreased water solubility owing to (i) the hydrophobicity of the chosen anchor and (ii) the increased molecular weight of the prodrug. With a suitably hydrophobic anchor, prodrugs may also be formed to make hydrophilic compounds water insoluble. The decreased water solubility of the prodrug enables nanoparticle formation in aqueous media via rapid precipitation.

For pharmaceutical applications, there are design constraints on the architecture of the prodrug, such as the chosen linker chemistry. While the Federal Code of Regulations Title 21 314.108 notes that attaching moieties to an active compound by chemistries that do not include the formation of an ester, salt or other noncovalent complex results in the formation of a new chemical entity, any covalent modification of a drug requires reevaluation of toxicity and efficacy. It is desirable that the original API be released from the prodrug via a degradable linkage to retain the therapeutic activity. Through various conjugation chemistries [54], the release half-life and release mechanism [55] may be modulated to tailor release on the hour of hours to days under desired environmental conditions.

Without conjugation, the anticancer drug paclitaxel has sufficient aqueous solubility to inhibit the formation of stable nanoparticles, even with the use of block copolymers. In a study by Saad and Ansell et al. a series of paclitaxel prodrugs were synthesized, varying the cross linking agent and the hydrophobicity of the anchor molecule, which enabled precipitation of block copolymer stabilized nanoparticles with diameters of 50–120 nm [30] and extended circulation half-lives of 24 h [56]. The release half-times were modulated between 1 and 24 h, depending on the hydrophobic anchor [56]. This is advantageous for stabilizing nanoparticles, controlling release and extending the therapeutic effects which is not possible for the unmodified drug, which rapidly partitions out of emulsion oil droplets on the order of minutes [56]. Similarly, Sengupta et al. tailored the precipitation of doxorubicin *via* conjugation to a hydrophobic poly (lactide-co-glycolide) polymer which was precipitated and stabilized with a phospholipid layer [57].

4.2. Ion pair formation to increase hydrophobicity

The formation of complexes driven by electrostatic interactions is an alternative to prodrugs which does not require chemical synthesis and is a well established technique for modulating solubility in the pharmaceutical industry. Hydrophobic ion pairs (HIP) are formed through a specific interaction with an oppositely charged molecule, which can reduce the solubility of ionic, peptide and protein APIs [58] by neutralizing the charge which facilitates solvation in aqueous media. HIPs may be pre-formed according to established procedures [59] and subsequently precipitated from organic media or may be

formed in-situ by reactive mixing to induce precipitation. While prior research on the formation of HIPs has been to improve drug permeability, intestinal absorption and to decrease dissolution rates [60], the typical complexes with logP values between 0 and 4 can result in HIP partitioning and destabilization of nanoparticles. Therefore, this technique is best applied through the choice of highly hydrophobic counter ions, such as long chain fatty acids as detailed by Stahl [59].

Similar techniques have been investigated for the precipitation of plasmid DNA and siRNA, which are vulnerable to degradation by polymerases and thus require protection for efficient delivery and transfection into cells [61]. The anionic charges on the phosphate backbone rapidly condense into polyplexes when in solution with cationic natural polymers [62], synthetic polymers [63,64] or lipids [65,66]. This is carried out in practice by mixing the two components in predetermined charge ratios, defined as the *N*/*P* ratio, where N = number of positive charges and P = number of negative charges. An excess of positive charge (high *N*/*P* ratio) is desirable to improve encapsulation or "trapping" of the drugs into the complex. A net charge on the resulting particles produces electrostatic stabilization in aqueous buffers *N*/*P* ratios closer to 1 may aggregate with time [62].

The condensation of DNA may proceed similarly to the nucleation and growth of organic nanoparticles, but there is very limited detailed work that has been conducted in this relatively new area of research. Using time-resolved multiangle laser light scattering, Lai and van Zanten have explored the effect of the *N*/*P* ratio on the condensation of plasmid DNA with poly-L-lysine, finding that at very high or very low *N*/*P*, the aggregate molecular mass is lower. The maximum sizes and densities were achieved at *N*/*P* near 1, which indicates that electrostatic stabilization is key in limiting extensive aggregation, through excess surface charge [67].

In contrast, success of siRNA condensation has been limited due to the smaller size and lower charge density when compared to plasmid DNA. Binding of siRNA to the polycation poly(ethyleneimine) (PEI) is 100 times weaker after administration *in vivo,* which leaves siRNA unbound and vulnerable to enzymatic attack [68]. To demonstrate the benefit of increased charge, modified siRNA "monomers" were polymerized through thiolated end groups and complexed with low molecular weight PEI, forming dense 235 nm spherical aggregates, in comparison to polydisperse, fractal objects yielded by complexation of "mono" siRNA to PEI [68].

4.3. Hydrophobic chelated radionuclide

Inorganic agents are useful in both chemotherapy [69] and the enhancement of *in vivo* imaging. Traditionally, these ions are complexed to low molecular weight chelating agents and are rapidly distributed systemically. Assembly of chelated radionuclides into particulate form holds the potential to achieve high loadings of cytotoxic radioactive agents into antibody targeted nanoparticles, which will improve localization and tumor eradiation. However, the traditional complexes which have been used are water soluble and generally have a net charge. Therefore, chemical modification is necessary to enable supersaturation in aqueous media and self assembly into a nanoparticle with extended circulation.

A number of synthetic routes may be pursued to arrive at a hydrophobic complex that can be self assembled *via* rapid precipitation, similar in concept to a therapeutic prodrug. Towards the design of a hydrophobic complex, DOTA has been conjugated to a cholesterol molecule, which eliminates one of the negatively charged carboxylic acid groups on the chelator, resulting in a net charge of −3 on the conjugate, which is neutralized upon reaction with Gd (III) [70]. In contrast, modifying DTPA with cholesterol renders a conjugate with a net −4 charge. Therefore, upon reaction with Gd (III) the final complex has a net negative charge and takes on amphiphilic character, self assembling into micellar structures with the chelated Gd exposed to the aqueous media [71].

5. Nanoparticle morphology

5.1. Effects of drug morphology

The morphology of a precipitated compound may change depending on the nucleation and growth kinetics—in fast processes, precipitation can effectively trap the drug in a less stable, high energy polymorph or amorphous phase in contrast to slower assembly or precipitation processes which yield thermodynamically stable polymorphs. On one hand, amorphous compounds offer significantly higher dissolution rates for hydrophobic compounds and, therefore, greater bioavailability. On the other hand, crystalline materials generally offer greater stability against degradation in storage. These factors must be balanced for a particular formulation.

While nanoparticles have enhanced dissolution kinetics over microparticles due to high surface to volume ratios (Section 6.3), drugs in amorphous form achieve higher supersaturations during dissolution owing to a higher chemical potential. A study of the solubility of bulk drugs in different crystal polymorphs and in amorphous form confirmed the increased drug solubility when in the amorphous form [72]. Oral administration of amorphous indomethacin capsules showed improved pharmacokinetics and *in vivo* absorption over the crystalline form, which correspond to the authors' findings of increased dissolution rate for the same drugs *in vitro* [73].

For the case of nanoparticles, high local concentrations of drug resulting from rapid dissolution may produce local drug concentrations above the MTD limit. A recent study directly compared the *in vitro* dissolution and *in vivo* bioavailability of crystalline and amorphous Itraconazole nanoparticles formed *via* wet milling and ultra rapid freezing processes, respectively [74]. Amorphous particles displayed an 8-fold increase in *in vitro* solution supersaturation and 4-fold increase in the bioavailability over crystalline nanoparticles. The implication of this study is that, in nanoparticle form, the crystalline or amorphous state of the drug still plays a key role in the observed bioavailability. More work in this area, including the administration of nanoparticles via alternate routes, is needed to further understand the effects of morphology on drug bioavailability. This result highlights the need to be able to determine the drug phase behavior and stability to achieve reproducible pharmacokinetic profiles.

5.2. Characterizing drug crystalline or amorphous state

Since the phase of the drug strongly influences its bioavailability, variation in nanoparticle composition over time is undesirable. This can occur by slow crystallization of amorphous phases and can alter release profiles and adversely affect the therapeutic effect of the formulation. There exist a number of useful techniques which have been developed to determine the state of bulk drug materials, such as X-ray diffraction, solid state NMR spectroscopy, differential scanning calorimetry and FTIR [75–78]; yet measurement becomes problematic when applied to nanoparticles, arising from reduced crystal length scales. For example, X-ray diffraction (XRD) for the characterization of crystal phases in nanoparticles often yields spectra with decreased signal and changes in relative intensities of characteristic crystal peaks after nanosizing. This has led researchers to conclude either that there is no change in crystal structure [39] or a decrease in crystal quality [40]. XRD has been applied to tracking the stability of drugs in solid lipid nanoparticles, where it was found that drug recrystallized from an amorphous state over time and manifested as expulsion of drug from the matrix upon storage [79]. Recently, Kumar, Adamson and Prud'homme [51] determined the crystallization or solubilization of

fluorescence probes in nanoparticle cores using fluorescence quenching, which revealed that the Flory–Huggins theory can be used to predict probe solubility or phase separation in the core of a nanoparticle. However, quantitative experimental assessment of the degree of crystallinity in nanoparticles cores remains a research challenge.

6. Particle stability

While a robust understanding of factors which influence nanoparticle formation and properties are essential to size control, equally as important are the colloidal stability and dissolution properties of the final suspension. As the size of particles is reduced, surface thermodynamics change and controlling the chemical and physical stability increases in difficulty. Here we briefly describe processes by which nanoparticles can undergo a loss of suspension stability, factors which influence nanoparticle dissolution, and stabilization and drying techniques, which are still an active area of research.

6.1. Nanoparticle stabilization

Irreversible aggregation of nanoparticles is caused by van der Waals interactions between particles. If there is no inherent surface charge, without stabilization *via* surface modification, aggregation of hydrophobic nanoparticles in aqueous media will occur soon after particle formation. Though nanoparticles can be stabilized *via* the adsorption of ionic surfactants or polymers in water, Zu et al. found that β-carotene nanoparticles stabilized by inherent surface charge or ε-polylysine were found to flocculate in a 1% saline solution [78]. Furthermore, research in the liposome literature has demonstrated a correlation between clearance times and the ability to bind protein [80,81], which is enhanced for highly charged surfaces. Hence, for *in vitro* and *in vivo* applications, particles with high surface charge are likely to flocculate at high salt concentrations or in the presence of blood proteins.

Surface modification *via* the addition of surface active molecules which create a steric barrier against aggregation, protein adsorption and macrophage clearance is an effective route towards stabilization of nanoparticles suspensions. It has been applied to "stealth" liposomes [82] and nanoparticles [14] with a PEG corona. Di-block [37], tri-block [36] and graft copolymers [83] have been used to coat nanoparticles through adsorption of blocky hydrophobic regions. Amphiphilic copolymers are particularly advantageous since the critical micelle concentration (CMC) is significantly lower than for surfactants. Furthermore, the larger hydrophobic segment of the molecule prevents the molecule from partitioning off of the nanoparticle surface *in vivo*. Amphiphilic polymers with multiple anchoring sites provide strong binding *via* cooperative multi-site attachment [84] but with the potential for aggregation through bridging interactions [84,85]. Diblock copolymers play a key role in both halting nanoparticle growth and stabilizing nanoparticle suspensions during rapid antisolvent precipitation because they are incapable of forming branched aggregates of nanoparticles [37,86].

6.2. Dissolution from nanoparticles

Many features of nanoparticles are common to larger crystals, but surface thermodynamics are not. We briefly summarize the key aspects which differentiate nanoparticle dissolution phenomenon, which becomes important after administration. For a spherical particle, the dissolution rate $\frac{dm}{dt}$ of a particle with radius r and mass m at time t is described by Fick's first law for diffusion [87]

$$\frac{dm}{dt} = -DA\frac{\partial c}{\partial r}\Big|_r \tag{8}$$

where D is the diffusion coefficient of the solute, A is the surface area of the particle, and $\frac{\partial c}{\partial r}|_r$ is the concentration gradient of the solute at the surface of the particle with radius r. The standard approach to model dissolution of a drug particle is to assume there is a thin "boundary layer" of thickness h surrounding the particle in which the steady state flux of the solute is constant and beyond which the concentration of drug is uniform and constant. For large crystals, the particle surface is approximated as a planar surface and a linear concentration gradient in the boundary layer applies. Due to the high radius of curvature, this approximation is not appropriate for dissolving nanoparticles under sink conditions. It can be shown that the appropriate concentration profile is given by [87]

$$\frac{\partial c}{\partial r} = c_s\left(\frac{1}{r} + \frac{1}{h}\right) \tag{9}$$

where c_s is the concentration at the particle surface. Therefore,

$$\frac{dm}{dt} = -DAc_s\left(\frac{1}{r} + \frac{1}{h}\right) \tag{10}$$

and the dissolution rate increases based on A and the inverse size dependence $\frac{1}{r}$.

For particles with diameters smaller than 200 nm, the thermodynamic solubility of the particle c_s in Eq. (10) is enhanced due to the high curvature at the particle interface according to the Kelvin equation [25,26],

$$c_s(r) = c_\infty\, exp\frac{2\gamma M}{\rho RTr} \tag{11}$$

where γ is the interfacial free energy, M is the molecular mass of the solute, ρ is the density, R is the gas constant, T is the absolute temperature, and c_∞ is the equilibrium solubility for a bulk material. The increased surface area and solubility enhance dissolution rates and have been demonstrated to increase the bioavailability of drugs that are difficult to deliver by oral tablets and capsules [16,17,88].

6.3. Ostwald ripening

Ostwald ripening is a slower process by which particle sizes shift during storage, driven by the suspension polydispersity and the solubility dependence on size. Though the particles may be protected against aggregation, when the particle size distribution is large, the smaller particles with increased solubility (Eq. (11)) shrink by dissolution and the drug subsequently precipitates on the surface of larger particles. The rate of this process is influenced by the chemical nature of the drug and the dispersity of the particle size distribution, a process which was modeled according to the average radius growth rate, derived by Lifshitz, Slyozov, and Wagner and quantitatively confirmed experimentally for a model system of β-carotene nanoparticles by Liu et al. [89].

6.4. Drying techniques

In addition to problems of colloidal stability and secondary recrystallization, aqueous suspensions of nanoparticles limit the concentrations of drugs that can be administered in a single dose, or require that a large volume dose be delivered to achieve the therapeutic concentration in circulation. As an alternative to liquid suspensions, storage of nanoparticles as dry powders enables both long term stability and the opportunity for drug concentration. Traditional drying techniques are not suitable for nanoparticles due to irreversible aggregation that occurs upon drying, which makes restoration of the original suspension by rehydration impossible.

Freeze drying and spray freeze drying are two viable techniques for obtaining dry powders of nanoparticles without extensive aggregation and are applicable to a number of therapeutic compounds. In freeze drying processes, water is removed from frozen nanoparticle suspensions by sublimation and desorption under high vacuum. Due to the stresses which are generated during freezing by the phase separation of pure water crystals and viscous concentrates containing nanoparticles, nanoparticles can be irreversibly fused or connected by interparticle bridging. To avoid these outcomes, cryoprotectants including carbohydrates like glucose, mannitol, sucrose and trehalose [86,90–92] and hydrophilic surfactants and polymers like polyvinyl alcohol [93], polyvinyl pyrrolidone (PVP) [94], Poloxamer 188 (Pluronic F68) [91], and hyrdoxypropyl methyl cellulose (HPMC) [95,96] have been used to form dry formulations. Combinations of carbohydrates and amphiphiles, such as trehalose and Poloxamer 188 [12,97], have been found to be more effective than the use of a single cryoprotectant. After nanoparticle formation, the presence of organic solvents can significantly hinder freeze drying and removal by vacuum or dialysis is necessary first.

Abdelwahed et al. have extensively reviewed cryoprotectants and methods for characterizing both dried and reconstituted powders [98]. Process parameters such as freezing rate and temperature, colloidal concentration, cyroprotectant type and concentration, drying time and temperature can affect the ease with which the dried powder can be resuspended back to the original size distribution. To resuspend freeze dried nanoparticles mechanical, sonic and thermal energy aid in the redispersion process. However, powders which may be sufficiently resuspended by simple shaking without the need for addition steps are ideal in a clinical setting.

Spray freeze drying has been applied in pharmaceutical research towards the development of therapeutic microparticles for inhalation [99–101] and to stabilize powders of proteins, often with the use of cryoprotectants in the formulation [99,101,102]. This technology has been translated to drying nanoparticle suspensions with and without cryoprotectants [86]. In spray freeze drying, the nanoparticle suspension is atomized and frozen in or over a cryogenic fluid, such as liquid nitrogen [103,104], which is advantageous since the reduced thermal mass of the droplets increases the cooling rate and can limit aggregation due to freezing stresses. Alternatives to freeze drying and spray freeze drying are techniques which flocculatete nanoparticles in a reversible fashion to facilitate filtration, enabling complete drying with reduced time and cost [86,105].

7. Conclusions

Advances in the development of new therapeutic agents have dictated the need for advanced delivery techniques and new API forms. The key to nanoparticle formation of APIs is the rapid and uniform imposition of high supersaturation to drive high nucleation rates. This kinetic control affords flexibility and enables high loadings of the API in nanoparticle form. The keys to controlling rapid precipitations are: (1) the control of micromixing in novel confined micromixers to afford supersaturations as large as 10^4 in milliseconds to initiate rapid nucleation of all components simultaneously, and (2) the balancing of particle growth rate with the adsorption kinetics of a stabilizing agent to arrest growth at a controlled size. An advantage of the continuous confined jet mixers is that they scale easily from laboratory experiments with a few milliliters to industrial scales with 10,000 L. While these precipitations can be effected for quite hydrophobic drug compounds, other techniques such as ionic complexation or conjugation must be employed to enable high supersaturations for less hydrophobic compounds. Post processing issues which must be addressed include the state of the drug—crystalline or amorphous—after the rapid precipitation, and recent advances in nanoparticle recovery make the preparation of redispersible nanoparticle formulations more promising. The move to more hydrophobic drug compounds and more active compounds makes the area of nanoparticle formulations particularly fertile for research and new process development.

References

[1] R.A. Petros, J.M. DeSimone, Strategies in the design of nanoparticles for therapeutic applications, Nat. Rev. Drug Discov. 9 (2010) 615–627.
[2] N.G. Khlebtsov, L.A. Dykman, Optical properties and biomedical applications of plasmonic nanoparticles, J. Quant. Spectrosc. Radiat. Transf. 111 (2010) 1–35.
[3] J. Zhou, Y. Sun, X.X. Du, L.Q. Xiong, H. Hu, F.Y. Li, Dual-modality in vivo imaging using rare-earth nanocrystals with near-infrared to near-infrared (NIR-to-NIR) upconversion luminescence and magnetic resonance properties, Biomaterials 31 (2010) 3287–3295.
[4] K. Kawabata, Y. Takakura, M. Hashida, The fate of plasmid DNA after intravenous-injection in mice—involvement of scavenger receptors in its hepatic-uptake, Pharm. Res. 12 (1995) 825–830.
[5] D.M. Dykxhoorn, D. Palliser, J. Lieberman, The silent treatment: siRNAs as small molecule drugs, Gene Ther. 13 (2006) 541–552.
[6] T.M. Allen, P.R. Cullis, Drug delivery systems: entering the mainstream, Science 303 (2004) 1818–1822.
[7] A. Carlmark, C.J. Hawker, A. Hult, M. Malkoch, New methodologies in the construction of dendritic materials, Chem. Soc. Rev. 38 (2009) 352–362.
[8] F. Szoka, D. Papahadjopoulos, Comparative properties and methods of preparation of lipid vesicles (liposomes), Annu. Rev. Biophys. Biol. 9 (1980) 467–508.
[9] R.H. Muller, K. Mader, S. Gohla, Solid lipid nanoparticles (SLN) for controlled drug delivery—a review of the state of the art, Eur. J. Pharm. Biol. 50 (2000) 161–177.
[10] C. Vauthier, K. Bouchemal, Methods for the preparation and manufacture of polymeric nanoparticles, Pharm. Res. 26 (2009) 1025–1058.
[11] Y. Liu, L. Huang, F. Liu, Paclitaxel nanocrystals for overcoming multidrug resistance in cancer, Mol. Pharm. 7 (2010) 863–869.
[12] V. Kumar, S.Y. Hong, A.E. Maciag, J.E. Saavedra, D.H. Adamson, R.K. Prud'homme, L.K. Keefer, H. Chakrapani, Stabilization of the nitric oxide (NO) prodrugs and anticancer leads, PABA/NO and double JS-K, through incorporation into PEG-protected nanoparticles, Mol. Pharm. 7 (2010) 291–298.
[13] L. Brannon-Peppas, J.O. Blanchette, Nanoparticle and targeted systems for cancer therapy, Adv. Drug Deliv. Rev. 56 (2004) 1649–1659.
[14] R. Gref, M. Luck, P. Quellec, M. Marchand, E. Dellacherie, S. Harnisch, T. Blunk, R.H. Muller, 'Stealth' corona-core nanoparticles surface modified by polyethylene glycol (PEG): influences of the corona (PEG chain length and surface density) and of the core composition on phagocytic uptake and plasma protein adsorption, Colloid. Surf. B 18 (2000) 301–313.
[15] V.C.F. Mosqueira, P. Legrand, A. Gulik, O. Bourdon, R. Gref, D. Labarre, G. Barratt, Relationship between complement activation, cellular uptake and surface physicochemical aspects of novel PEG-modified nanocapsules, Biomaterials 22 (2001) 2967–2979.
[16] M.H. El-Shabouri, Nanoparticles for improving the dissolution and oral bioavailability of spironolactone, a poorly-soluble drug, Stp Pharm. Sci. 12 (2002) 97–101.
[17] G.G. Liversidge, K.C. Cundy, Particle-size reduction for improvement of oral bioavailability of hydrophobic drugs.1. Absolute oral bioavailability of nanocrystalline danazol in beagle dogs, Int. J. Pharm. 125 (1995) 91–97.
[18] H. Maeda, J. Wu, T. Sawa, Y. Matsumura, K. Hori, Tumor vascular permeability and the EPR effect in macromolecular therapeutics: a review, J. Control. Release 65 (2000) 271–284.
[19] Y. Matsumura, H. Maeda, A new concept for macromolecular therapeutics in cancer-chemotherapy—mechanism of tumoritropic accumulation of proteins and the antitumor agent smancs, Cancer Res. 46 (1986) 6387–6392.
[20] S.T. Reddy, A.J. van der Vlies, E. Simeoni, V. Angeli, G.J. Randolph, C.P. O'Neill, L.K. Lee, M.A. Swartz, J.A. Hubbell, Exploiting lymphatic transport and complement activation in nanoparticle vaccines, Nat. Biotechnol. 25 (2007) 1159–1164.
[21] R. Langer, Drug delivery and targeting, Nature 392 (1998) 5–10.
[22] E. Merisko-Liversidge, G.G. Liversidge, E.R. Cooper, Nanosizing: a formulation approach for poorly-water-soluble compounds, Eur. J. Pharm. Sci. 18 (2003) 113–120.
[23] J.W. Mullin, Mechanism of Crystallisation, Crystallisation, Butterworth & Co. Ltd., London, 1972, p. 142.
[24] J.W. Mullin, Mechanism of Crystallisation, Crystallisation, Butterworth & Co. Ltd., London, 1972, p. 140.
[25] L.F. Knapp, The solubility of small particles and the stability of colloids, T. Faraday Soc. 17 (1922) 457–465.
[26] L.M. Skinner, J.R. Sambles, The Kelvin equation—a review, Aerosol Sci. 3 (1972) 199–210.
[27] M.C. Brick, H.J. Palmer, T.H. Whitesides, Formation of colloidal dispersions of organic materials in aqueous media by solvent shifting, Langmuir 19 (2003) 6367–6380.
[28] J.W. Mullin, Crystallization Kinetics, Crystallization, Butterworth & Co. Ltd., London, 1972, pp. 178–185.
[29] J.W. Mullin, Mechanism of Crystallization, Crystallization, Butterworth & Co. Ltd, London, 1972, pp. 146–150.
[30] W. Saad, Drug Nanoparticle Formation via Flash NanoPrecipitation: Conjugation to Encapsulate and Control the Release of Paclitaxel, Chemical Engineering, Princeton University, Princeton, 2007.

[31] A.J. Mahajan, D.J. Kirwan, Nucleation and growth-kinetics of biochemicals measured at high supersaturations, J. Cryst. Growth 144 (1994) 281–290.
[32] A.G. Jones, J.W. Mullin, Programmed cooling crystallization of potassium sulfate solutions, Chem. Eng. Sci. 29 (1974) 105–118.
[33] J. Worlitschek, M. Mazzotti, Model-based optimization of particle size distribution in batch-cooling crystallization of paracetamol, Cryst. Growth Des. 4 (2004) 891–903.
[34] J.W. Chew, S.N. Black, P.S. Chow, R.B.H. Tan, Comparison between open-loop temperature control and closed-loop supersaturation control for cooling crystallization of glycine, Ind. Eng. Chem. Res. 46 (2007) 830–838.
[35] S.D. Durbin, G. Feher, Crystal-growth studies of lysozyme as a model for protein crystallization, J. Cryst. Growth 76 (1986) 583–592.
[36] V. Kumar, L. Wang, M. Riebe, H.H. Tung, R.K. Prud'homme, Formulation and stability of ltraconazole and odanacatib nanoparticles: governing physical parameters, Mol. Pharm. 6 (2009) 1118–1124.
[37] B.K. Johnson, R.K. Prud'homme, Flash nanoprecipitation of organic actives and block copolymers using a confined impinging jets mixer, Aust. J. Chem. 56 (2003) 1021–1024.
[38] M.E. Matteucci, M.A. Hotze, K.P. Johnston, R.O. Williams, Drug nanoparticles by antisolvent precipitation: mixing energy versus surfactant stabilization, Langmuir 22 (2006) 8951–8959.
[39] H. Zhao, J.X. Wang, Q.A. Wang, J.F. Chen, J. Yun, Controlled liquid antisolvent precipitation of hydrophobic pharmaceutical nanoparticles in a microchannel reactor, Ind. Eng. Chem. Res. 46 (2007) 8229–8235.
[40] M. Kakran, N.G. Sahoo, L. Li, Z. Judeh, Y. Wang, K. Chong, L. Loh, Fabrication of drug nanoparticles by evaporative precipitation of nanosuspension, Int. J. Pharm. 383 (2010) 285–292.
[41] U. Bilati, E. Allemann, E. Doelker, Development of a nanoprecipitation method intended for the entrapment of hydrophilic drugs into nanoparticles, Eur. J. Pharm. Sci. 24 (2005) 67–75.
[42] B.K. Nyambura, I.W. Kellaway, K.M.G. Taylor, The processing of nanoparticles containing protein for suspension in hydrofluoroalkane propellants, Int. J. Pharm. 372 (2009) 140–146.
[43] B.K. Johnson, R.K. Prud'homme, Chemical processing and micromixing in confined impinging jets, AIChE J. 49 (2003) 2264–2282.
[44] M.R. Aberturas, J. Molpeceres, M. Guzman, F. Garcia, Development of a new cyclosporine formulation based on poly(caprolactone) microspheres, J. Microencapsul. 19 (2002) 61–72.
[45] J. Cheng, B.A. Teply, I. Sherifi, J. Sung, G. Luther, F.X. Gu, E. Levy-Nissenbaum, A.F. Radovic-Moreno, R. Langer, O.C. Farokhzad, Formulation of functionalized PLGA-PEG nanoparticles for in vivo targeted drug delivery, Biomaterials 28 (2007) 869–876.
[46] Y. Liu, R.O. Fox, CFD predictions for chemical processing in a confined impinging-jets reactor, AIChE J. 52 (2006) 731–744.
[47] S. Mawson, S. Kanakia, K.P. Johnston, Coaxial nozzle for control of particle morphology in precipitation with a compressed fluid antisolvent, J. Appl. Polym. Sci. 64 (1997) 2105–2118.
[48] Y. Liu, C.Y. Cheng, Y. Liu, R.K. Prud'homme, R.O. Fox, Mixing in a multi-inlet vortex mixer (MIVM) for flash nano-precipitation, Chem. Eng. Sci. 63 (2008) 2829–2842.
[49] T. Chen, S.M. D'Addio, M.T. Kennedy, A. Swietlow, I.G. Kevrekidis, A.Z. Panagiotopoulos, R.K. Prud'homme, Protected peptide nanoparticles: experiments and brownian dynamics simulations of the energetics of assembly, Nano Lett. 9 (2009) 2218–2222.
[50] M. Akbulut, P. Ginart, M.E. Gindy, C. Theriault, K.H. Chin, W. Soboyejo, R.K. Prud'homme, Generic method of preparing multifunctional fluorescent nanoparticles using flash nanoprecipitation, Adv. Funct. Mater. 19 (2009) 718–725.
[51] V. Kumar, D.H. Adamson, R.K. Prud'homme, Fluorescent polymeric nanoparticles: aggregation and phase behavior of pyrene and amphotericin B molecules in nanoparticle cores, Small 6 (2010) 2907–2914.
[52] S.J. Budijono, J.N. Shan, N. Yao, Y. Miura, T. Hoye, R.H. Austin, Y.G. Ju, R.K. Prud'homme, Synthesis of stable block-copolymer-protected NaYF4:Yb3+, Er3+ Up-converting phosphor nanoparticles, Chem. Mater. 22 (2010) 311–318.
[53] M.E. Gindy, A.Z. Panagiotopoulos, R.K. Prud'homme, Composite block copolymer stabilized nanoparticles: simultaneous encapsulation of organic actives and inorganic nanostructures, Langmuir 24 (2008) 83–90.
[54] J. Rautio, H. Kumpulainen, T. Heimbach, R. Oliyai, D. Oh, T. Jarvinen, J. Savolainen, Prodrugs: design and clinical applications, Nat. Rev. Drug Discov. 7 (2008) 255–270.
[55] A.J.M. D'Souza, E.M. Topp, Release from polymeric prodrugs: linkages and their degradation, J. Pharm. Sci. 93 (2004) 1962–1979.
[56] S.M. Ansell, S.A. Johnstone, P.G. Tardi, L. Lo, S.W. Xie, Y. Shu, T.O. Harasym, N.L. Harasym, L. Williams, D. Bermudes, B.D. Liboiron, W. Saad, R.K. Prud'homme, L.D. Mayer, Modulating the therapeutic activity of nanoparticle delivered paclitaxel by manipulating the hydrophobicity of prodrug conjugates, J. Med. Chem. 51 (2008) 3288–3296.
[57] S. Sengupta, D. Eavarone, I. Capila, G.L. Zhao, N. Watson, T. Kiziltepe, R. Sasisekharan, Temporal targeting of tumour cells and neovasculature with a nanoscale delivery system, Nature 436 (2005) 568–572.
[58] J.D. Meyer, M.C. Manning, Hydrophobic ion pairing: altering the solubility properties of biomolecules, Pharm. Res. 15 (1998) 188–193.
[59] Handbook of Pharmaceutical Salts: Properties, Selection, and Use, Verlag Helvetica Chimica Aeta, Zurich, 2008.
[60] J.M. Miller, A. Dahan, D. Gupta, S. Varghese, G.L. Amidon, Enabling the intestinal absorption of highly polar antiviral agents: ion-pair facilitated membrane permeation of zanamivir heptyl ester and guanidino oseltamivir, Mol. Pharm. 7 (2010) 1223–1234.
[61] J. Soutschek, A. Akinc, B. Bramlage, K. Charisse, R. Constien, M. Donoghue, S. Elbashir, A. Geick, P. Hadwiger, J. Harborth, M. John, V. Kesavan, G. Lavine, R.K. Pandey, T. Racie, K.G. Rajeev, I. Rohl, I. Toudjarska, G. Wang, S. Wuschko, D. Bumcrot, V. Koteliansky, S. Limmer, M. Manoharan, H.P. Vornlocher, Therapeutic silencing of an endogenous gene by systemic administration of modified siRNAs, Nature 432 (2004) 173–178.
[62] J.M. Dang, K.W. Leong, Natural polymers for gene delivery and tissue engineering, Adv. Drug Deliv. Rev. 58 (2006) 487–499.
[63] D.W. Pack, A.S. Hoffman, S. Pun, P.S. Stayton, Design and development of polymers for gene delivery, Nat. Rev. Drug Discov. 4 (2005) 581–593.
[64] M.J. Tiera, F.M. Winnik, J.C. Fernandes, Synthetic and natural polycations for gene therapy: state of the art and new perspectives, Curr. Gene Ther. 6 (2006) 59–71.
[65] S. Hirota, C.T. de Ilarduya, L.G. Barron, F.C. Szoka, Simple mixing device to reproducibly prepare cationic lipid-DNA complexes (lipoplexes), Biotechniques 27 (1999) 286–289.
[66] S.C. Semple, A. Akinc, J.X. Chen, A.P. Sandhu, B.L. Mui, C.K. Cho, D.W.Y. Sah, D. Stebbing, E.J. Crosley, E. Yaworski, I.M. Hafez, J.R. Dorkin, J. Qin, K. Lam, K.G. Rajeev, K.F. Wong, L.B. Jeffs, L. Nechev, M.L. Eisenhardt, M. Jayaraman, M. Kazem, M.A. Maier, M. Srinivasulu, M.J. Weinstein, Q.M. Chen, R. Alvarez, S.A. Barros, S. De, S.K. Klimuk, T. Borland, V. Kosovrasti, W.L. Cantley, Y.K. Tam, M. Manoharan, M.A. Ciufolini, M.A. Tracy, A. de Fougerolles, I. MacLachlan, P.R. Cullis, T.D. Madden, M.J. Hope, Rational design of cationic lipids for siRNA delivery, Nat. Biotechnol. 28 (2010) 172–176.
[67] E. Lai, J.H. van Zanten, Monitoring DNA/poly-L-lysine polyplex formation with time-resolved multiangle laser light scattering, Biophys. J. 80 (2001) 864–873.
[68] S.Y. Lee, M.S. Huh, S. Lee, S.J. Lee, H. Chung, J.H. Park, Y.K. Oh, K. Choi, K. Kim, I.C. Kwon, Stability and cellular uptake of polymerized siRNA (poly-siRNA)/polyethylenimine (PEI) complexes for efficient gene silencing, J. Control. Release 141 (2010) 339–346.
[69] M.R. McDevitt, D.S. Ma, L.T. Lai, J. Simon, P. Borchardt, R.K. Frank, K. Wu, V. Pellegrini, M.J. Curcio, M. Miederer, N.H. Bander, D.A. Scheinberg, Tumor therapy with targeted atomic nanogenerators, Science 294 (2001) 1537–1540.
[70] M. Oliver, A. Ahmad, N. Kamaly, E. Perouzel, A. Caussin, M. Keller, A. Herlihy, J. Bell, A.D. Miller, M.R. Jorgensen, MAGfect: a novel liposome formulation for MRI labelling and visualization of cells, Org. Biomol. Chem. 4 (2006) 3489–3497.
[71] L. Lattuada, G. Lux, Synthesis of Gd-DTPA-cholesterol: a new lipophilic gadolinium complex as a potential MRI contrast agent, Tetrahedron Lett. 44 (2003) 3893–3895.
[72] B.C. Hancock, M. Parks, What is the true solubility advantage for amorphous pharmaceuticals? Pharm. Res. 17 (2000) 397–404.
[73] E. Fukuoka, M. Makita, S. Yamamura, Glassy state of pharmaceuticals. II. Bioinequivalence of glassy and crystalline indomethacin, Chem. Pharm. Bull. 35 (1987) 2943–2948.
[74] W. Yang, K.P. Johnston, R.O. Williams, Comparison of bioavailability of amorphous versus crystalline itraconazole nanoparticles via pulmonary administration in rats, Eur. J. Pharm. Biopharm. 75 (2010) 33–41.
[75] Y. Hu, X.Q. Jiang, Y. Ding, L.Y. Zhang, C.Z. Yang, J.F. Zhang, J.N. Chen, Y.H. Yang, Preparation and drug release behaviors of nimodipine-loaded poly(caprolactone)-poly(ethylene oxide)-polylactide amphiphilic copolymer nanoparticles, Biomaterials 24 (2003) 2395–2404.
[76] D.M. Schachter, J.C. Xiong, G.C. Tirol, Solid state NMR perspective of drug-polymer solid solutions: a model system based on poly(ethylene oxide), Int. J. Pharm. 281 (2004) 89–101.
[77] C.A. Coutts-Lendon, N.A. Wright, E.V. Mieso, J.L. Koenig, The use of FT-IR imaging as an analytical tool for the characterization of drug delivery systems, J. Control. Release 93 (2003) 223–248.
[78] Z.X. Zhu, K. Margulis-Goshen, S. Magdassi, Y. Talmon, C.W. Macosko, Polyelectrolyte stabilized drug nanoparticles via flash nanoprecipitation: a model study with beta-carotene, J. Pharm. Sci. 99 (2010) 4295–4306.
[79] J. Pietkiewicz, M. Sznitowska, M. Placzek, The expulsion of lipophilic drugs from the cores of solid lipid microspheres in diluted suspensions and in concentrates, Int. J. Pharm. 310 (2006) 64–71.
[80] A. Chonn, S.C. Semple, P.R. Cullis, Association of blood proteins with large unilamellar liposomes invivo—relation to circulation lifetimes, J. Biol. Chem. 267 (1992) 18759–18765.
[81] J.H. Senior, Fate and behavior of liposomes invivo—a review of controlling factors, Crit. Rev. Therm. Drug 3 (1987) 123–193.
[82] D.D. Lasic, D. Needham, The "stealth" liposome: a prototypical biomaterial, Chem. Rev. 95 (1995) 2601–2628.
[83] T. Akagi, T. Kaneko, T. Kida, M. Akashi, Multifunctional conjugation of proteins on/into bio-nanoparticles prepared by amphiphilic poly(gamma-glutamic acid), J. Biomater. Sci. Polym. Ed. 17 (2006) 875–892.
[84] D.T. Auguste, R.K. Prud'homme, P.L. Ahl, P. Meers, J. Kohn, Association of hydrophobically-modified poly(ethylene glycol) with fusogenic liposomes, BBA-Biomembranes 1616 (2003) 184–195.
[85] H.S. Ashbaugh, K. Boon, R.K. Prud'homme, Gelation of "catanionic" vesicles by hydrophobically modified polyelectrolytes, Colloid Polym. Sci. 280 (2002) 783–788.
[86] S.M. D'Addio, C. Kafka, M. Akbulut, P. Beattie, W. Saad, M. Herrera, M.T. Kennedy, R.K. Prud'homme, Novel method for concentrating and drying polymeric nanoparticles: hydrogen bonding coacervate precipitation, Mol. Pharm. 7 (2010) 557–564.
[87] J.Z. Wang, D.R. Flanagan, General solution for diffusion controlled dissolution of spherical particles. 1. Theory, J. Pharm. Sci. 88 (1999) 731–738.
[88] W.K. Kraft, B. Steiger, D. Beussink, J.N. Quiring, N. Fitzgerald, H.E. Greenberg, S.A. Waldman, The pharmacokinetics of nebulized nanocrystal budesonide suspension in healthy volunteers, J. Clin. Pharmacol. 44 (2004) 67–72.

[89] Y. Liu, K. Kathan, W. Saad, R.K. Prud'homme, Ostwald ripening of beta-carotene nanoparticles, Phys. Rev. Lett. 98 (2007) 036102.
[90] S. de Chasteigner, G. Cave, H. Fessi, J.P. Devissaguet, F. Puisieux, Freeze-drying of itraconazole-loaded nanosphere suspensions: a feasibility study, Drug Dev. Res. 38 (1996) 116–124.
[91] R. Cavalli, O. Caputo, M.E. Carlotti, M. Trotta, C. Scarnecchia, M.R. Gasco, Sterilization and freeze-drying of drug-free and drug-loaded solid lipid nanoparticles, Int. J. Pharm. 148 (1997) 47–54.
[92] Y.I. Jeong, Y.H. Shim, C. Kim, G.T. Lim, K.C. Choi, C. Yoon, Effect of cryoprotectants on the reconstitution of surfactant-free nanoparticles of poly(DL-lactide-co-glycolide), J. Microencapsul. 22 (2005) 593–601.
[93] W. Abdelwahed, G. Degobert, H. Fessi, A pilot study of freeze drying of poly (epsilon-caprolactone) nanocapsules stabilized by poly(vinyl alcohol): formulation and process optimization, Int. J. Pharm. 309 (2006) 178–188.
[94] T.L. Rogers, I.B. Gillespie, J.E. Hitt, K.L. Fransen, C.A. Crowl, C.J. Tucker, G.B. Kupperblatt, J.N. Becker, D.L. Wilson, C. Todd, E.J. Elder, Development and characterization of a scalable controlled precipitation process to enhance the dissolution of poorly water-soluble drugs, Pharm. Res. 21 (2004) 2048–2057.
[95] M.E. Matteucci, B.K. Brettmann, T.L. Rogers, E.J. Elder, R.O. Williams, K.P. Johnston, Design of potent amorphous drug nanoparticles for rapid generation of highly supersaturated media, Mol. Pharm. 4 (2007) 782–793.
[96] M.E. Matteucci, J.C. Paguio, M.A. Miller, R.O. Williams, K.P. Johnston, Flocculated amorphous nanoparticles for highly supersaturated solutions, Pharm. Res. 25 (2008) 2477–2487.
[97] A.M. Layre, P. Couvreur, J. Richard, D. Requier, N.E. Ghermani, R. Gref, Freeze-drying of composite core-shell nanoparticles, Drug Dev. Ind. Pharm. 32 (2006) 839–846.
[98] W. Abdelwahed, G. Degobert, S. Stainmesse, H. Fessi, Freeze-drying of nanoparticles: formulation, process and storage considerations, Adv. Drug Deliv. Rev. 58 (2006) 1688–1713.
[99] Y.F. Maa, P.A. Nguyen, T. Sweeney, S.J. Shire, C.C. Hsu, Protein inhalation powders: spray drying vs spray freeze drying, Pharm. Res. 16 (1999) 249–254.
[100] L.G. Sweeney, Z.L. Wang, R. Loebenberg, J.P. Wong, C.F. Lange, W.H. Finlay, Spray-freeze-dried liposomal ciprofloxacin powder for inhaled aerosol drug delivery, Int. J. Pharm. 305 (2005) 180–185.
[101] S. Azarmi, R. Lobenberg, W.H. Roa, S.S. Tai, W.H. Finlay, Formulation and in vivo evaluation of effervescent inhalable carrier particles for pulmonary delivery of nanoparticles, Drug Dev. Ind. Pharm. 34 (2008) 943–947.
[102] S.D. Webb, S.L. Golledge, J.L. Cleland, J.F. Carpenter, T.W. Randolph, Surface adsorption of recombinant human interferon-gamma in lyophilized and spray-lyophilized formulations, J. Pharm. Sci. 91 (2002) 1474–1487.
[103] Z.S. Yu, K.P. Johnston, R.O. Williams, Spray freezing into liquid versus spray-freeze drying: influence of atomization on protein aggregation and biological activity, Eur. J. Pharm. Sci. 27 (2006) 9–18.
[104] M.T. Kennedy, A. Ali-Reynolds, C. Farrier, P.A. Burke, Atomizing into a chilled extraction solvent eliminates liquid gas from a spray-freeze drying microencapsulation process, J. Pharm. Sci. 97 (2008) 4459–4472.
[105] X.X. Chen, M.E. Matteucci, C.Y. Lo, K.P. Johnston, R.O. Williams, Flocculation of polymer stabilized nanocrystal suspensions to produce redispersible powders, Drug Dev. Ind. Pharm. 35 (2009) 283–296.
[106] R.J. Demyanovich, J.R. Bourne, Rapid micromixing by the impingement of thin liquid sheets. II. Mixing study, Ind. Eng. Chem. Res. 28 (1989) 830–839.
[107] J.R. Bourne, J. Lenzner, S. Petrozzi, Micromixing in static mixers—an experimental-study, Ind. Eng. Chem. Res. 31 (1992) 1216–1222.
[108] J.R. Bourne, M. Studer, Fast reactions in rotor-stator mixers of different size, Chem. Eng. Process. 31 (1992) 285–296.
[109] J. Baldyga, J.R. Bourne, B. Dubuis, A.W. Etchells, R.V. Gholap, B. Zimmermann, Jet reactor scale-up for mixing-controlled reactions, Chem. Eng. Res. Des. 73 (1995) 497–502.